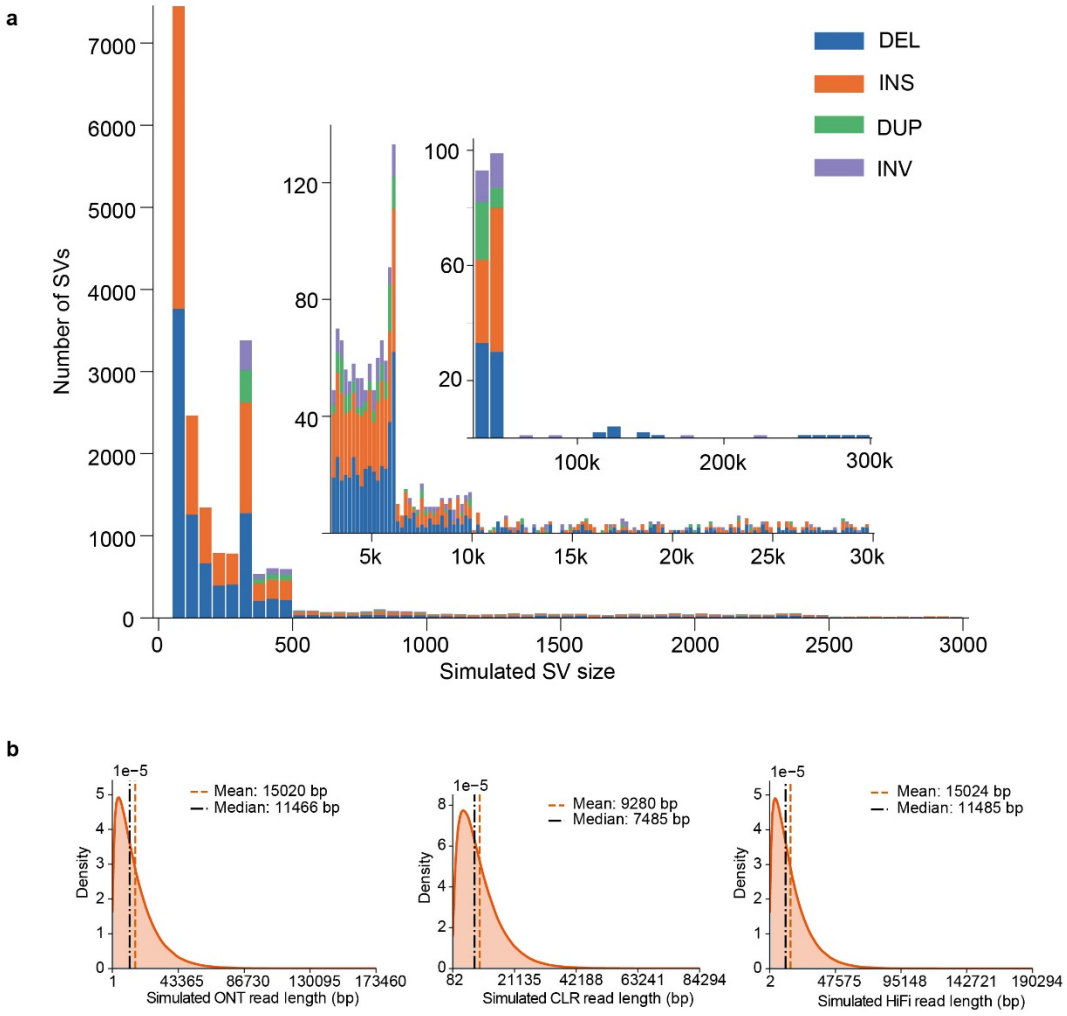

Supplementary Figure 1. **Simulated SVs and read length distributions**. **a,** Size distribution of simulated SVs. The peak at 300–400 bp corresponds to simulated *Alu* elements, whereas the peak at ~6 kb represents mobile elements. **b,** Length distributions of simulated ONT, CLR, and HiFi reads.

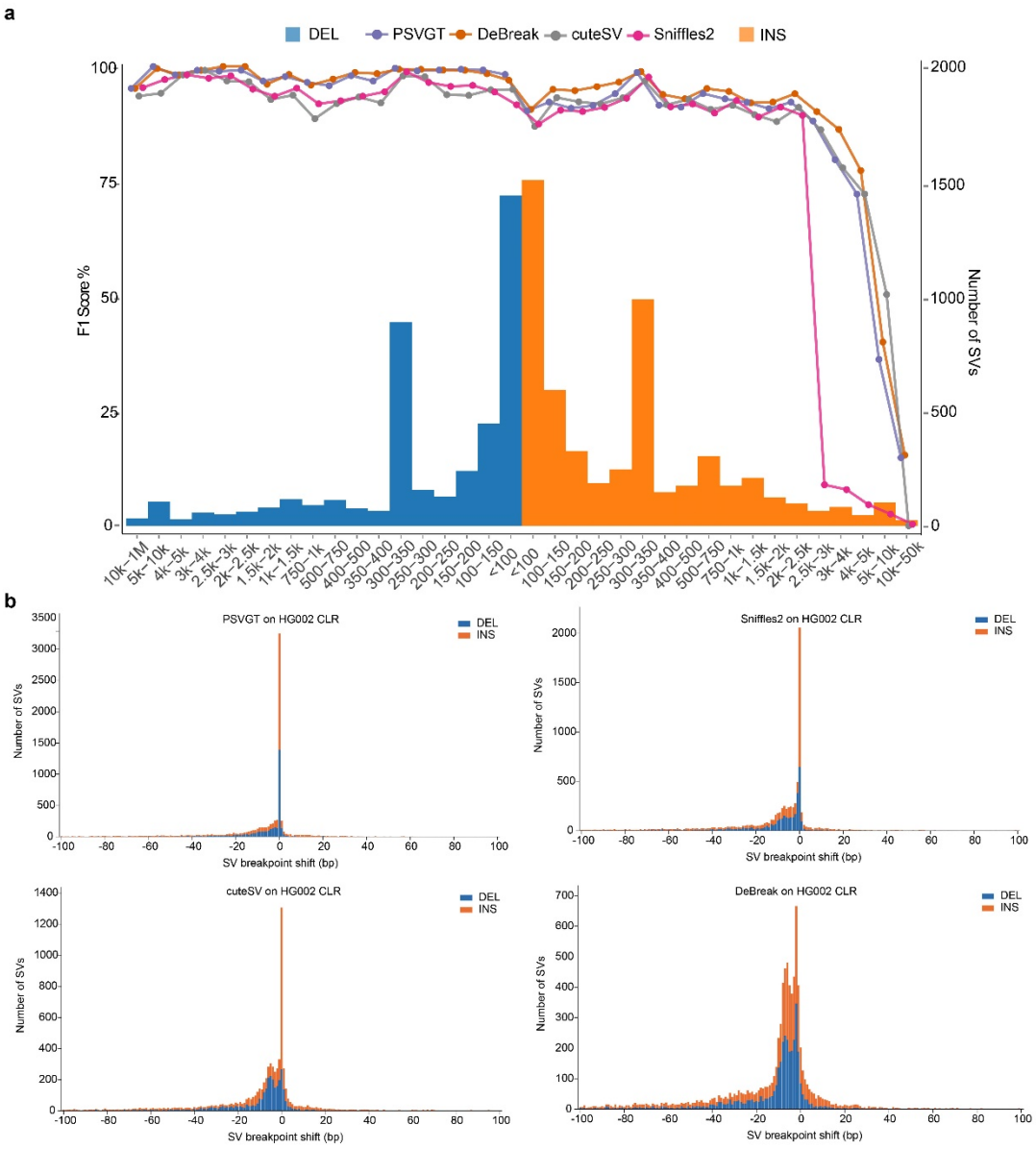

Supplementary Figure 2. **Benchmarking SV detection accuracy on PacBio CLR datasets from HG002**. **a,** F1 score distribution across SV size ranges. Colored lines indicate the F1 scores of the evaluated SV callers, whereas the bar plots show the corresponding size distribution of SVs. **b,** Breakpoint accuracy for the four callers on HG002 CLR datasets; SVs with breakpoint shift ≤ 100 bp were considered.

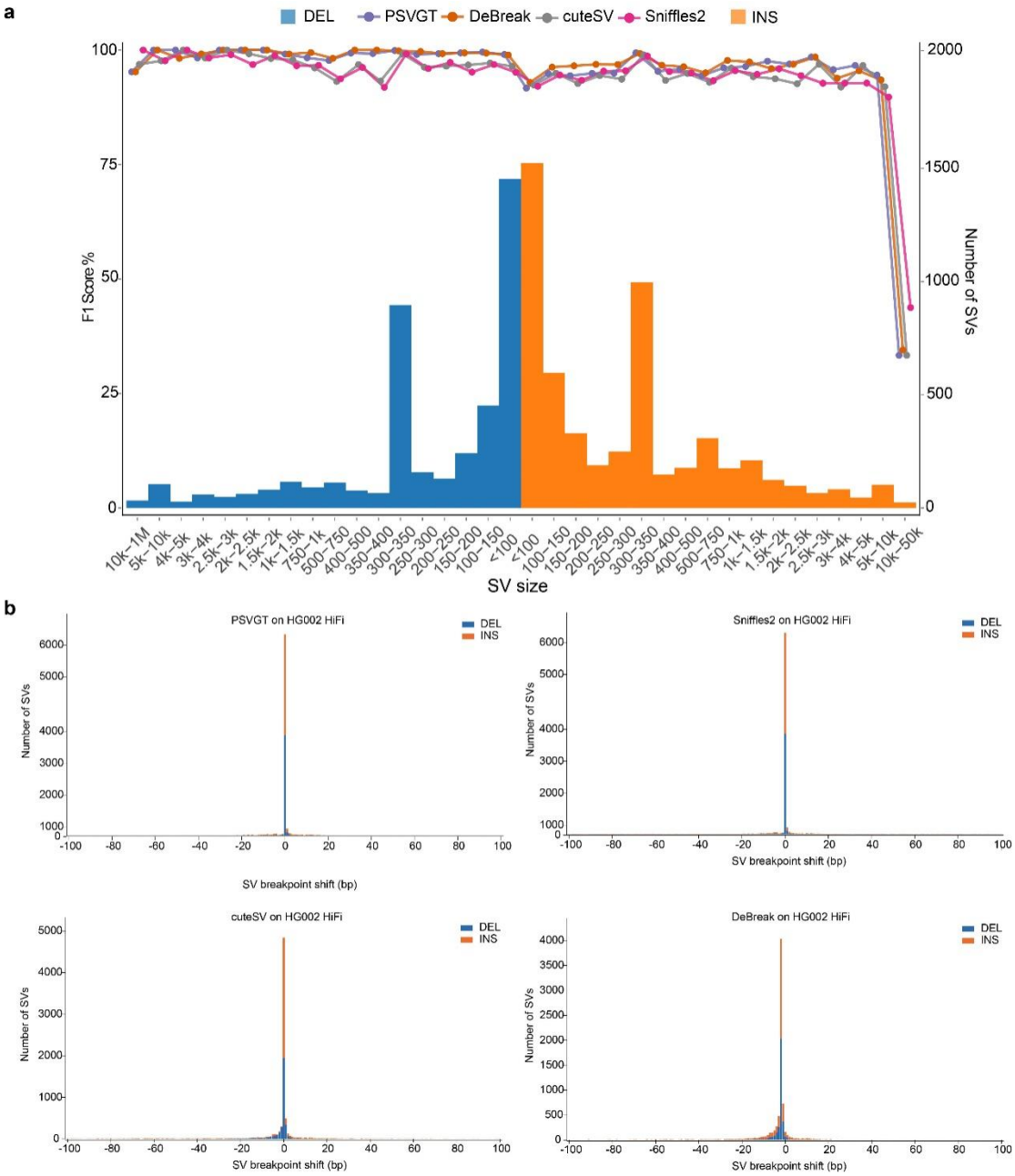

Supplementary Figure 3. **Benchmarking SV detection accuracy on PacBio HiFi datasets from HG002**. **a,** F1 score distribution across SV size ranges. Colored lines indicate the F1 scores of the evaluated callers, whereas the bar plots show the corresponding size distribution of SVs. **b,** Breakpoint accuracy for the four callers on HG002 HiFi datasets; SVs with breakpoint shift ≤ 100 bp were considered.

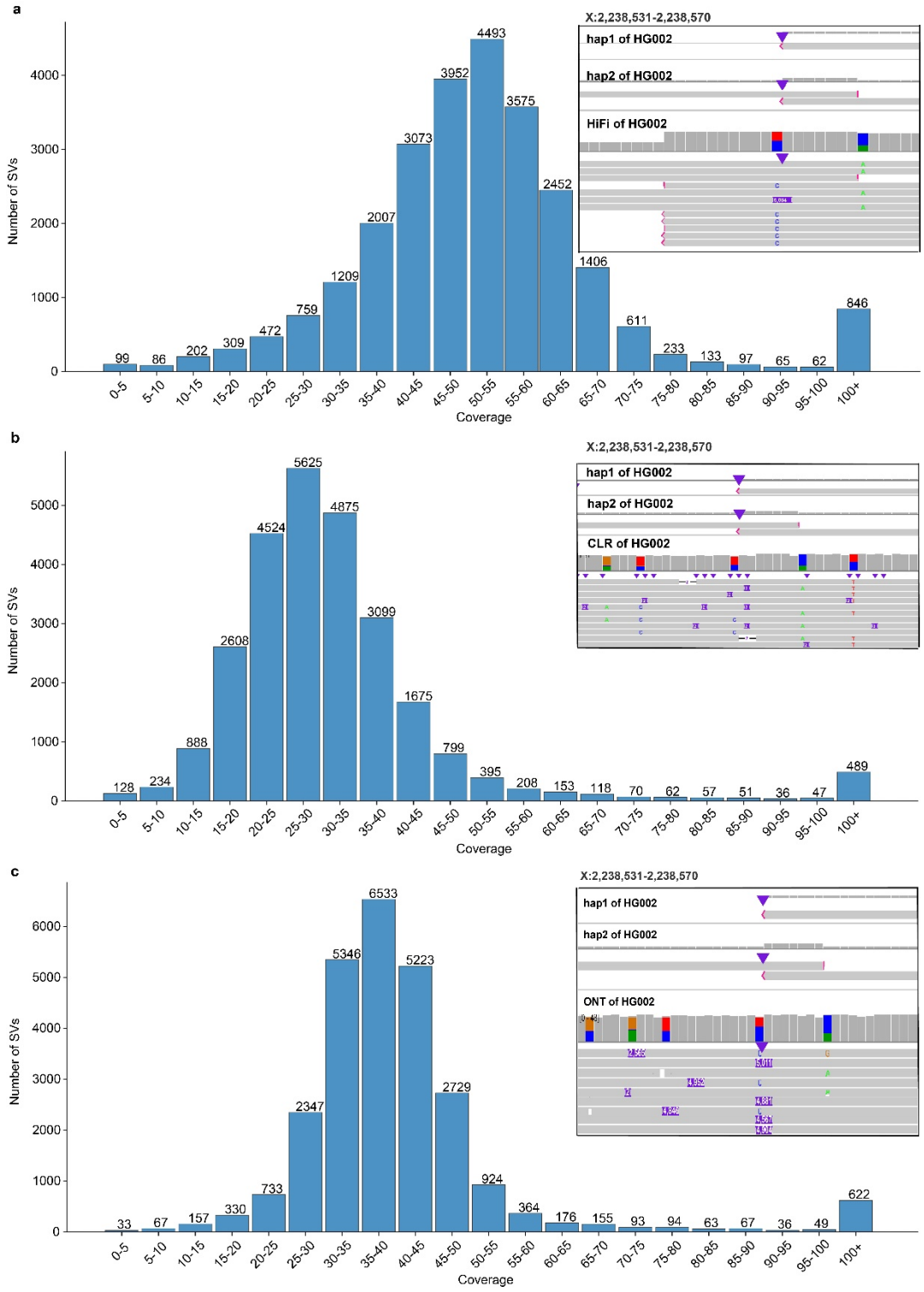

Supplementary Figure 4. **Local coverage distribution of SVs in HG002. a-c,** Local coverage profiles of SVs detected from PacBio HiFi **(a)**, PacBio CLR **(b)**, and ONT **(c)** datasets. Representative IGV snapshots illustrate a 5,071-bp insertion at locus X:2,238,531–2,238,570. Insertion-related CIGAR operations are highlighted in purple triangle.

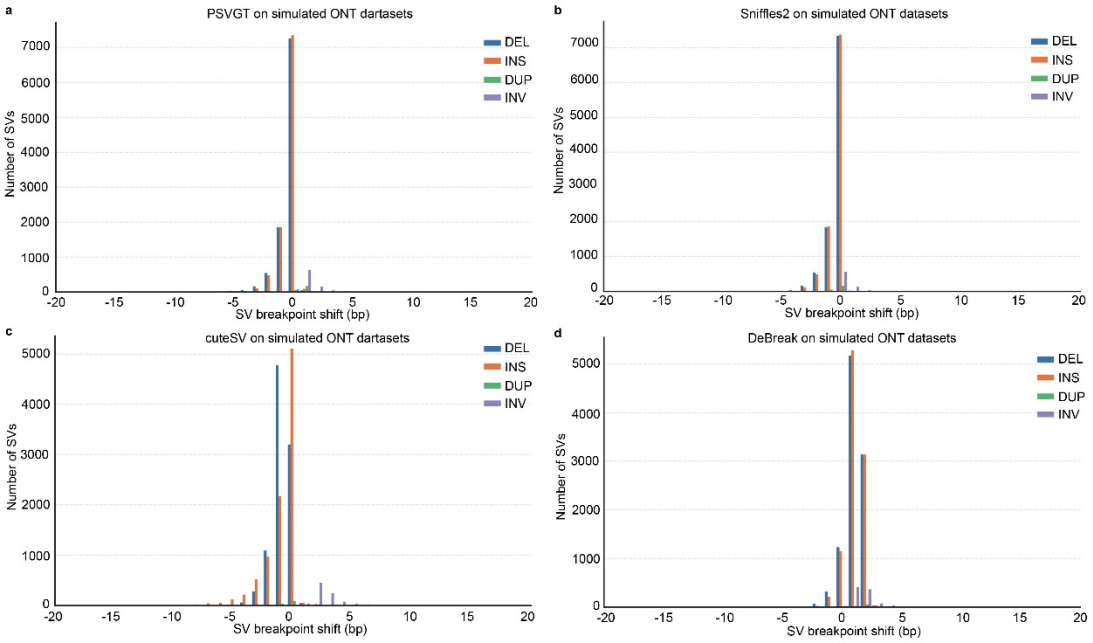

Supplementary Figure 5. **Breakpoint accuracy of SVs detected from ONT datasets. a-d,** Breakpoint accuracy for PSVGT **(a)**, Sniffles2 **(b)**, cuteSV **(c)**, and DeBreak **(d)**. SVs with breakpoint shift ≤ 20 bp are displayed.

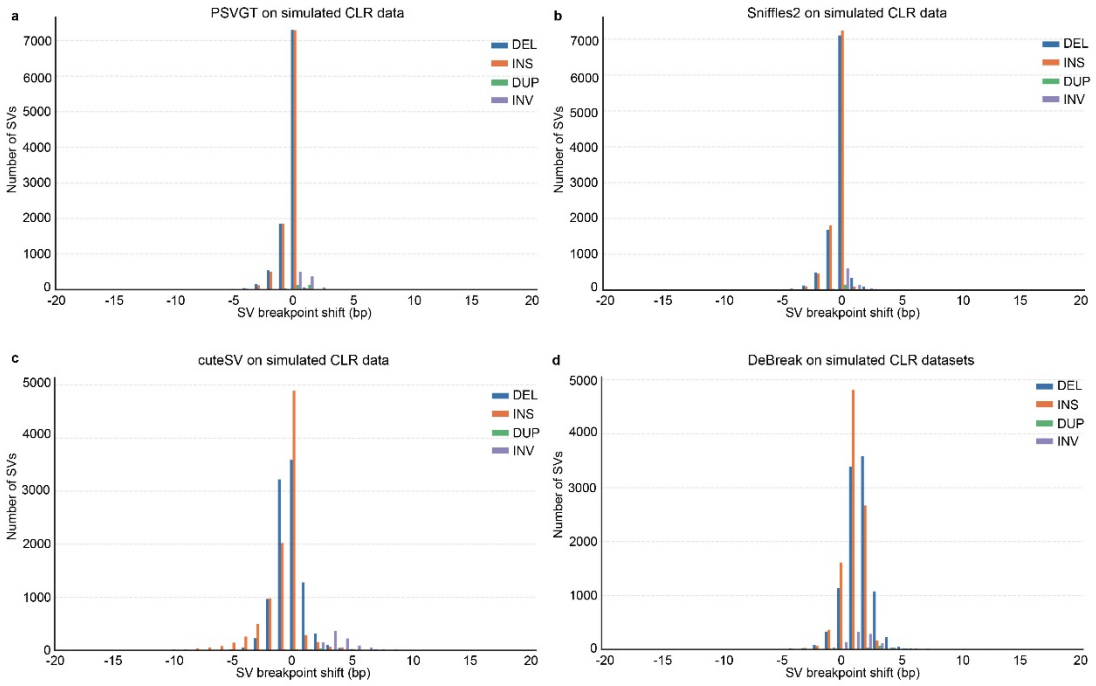

Supplementary Figure 6. **Breakpoint accuracy of SVs detected from CLR datasets. a-d,** Breakpoint accuracy for PSVGT **(a)**, Sniffles2 **(b)**, cuteSV **(c)**, and DeBreak **(d)**. SVs with breakpoint shift ≤ 20 bp are displayed.

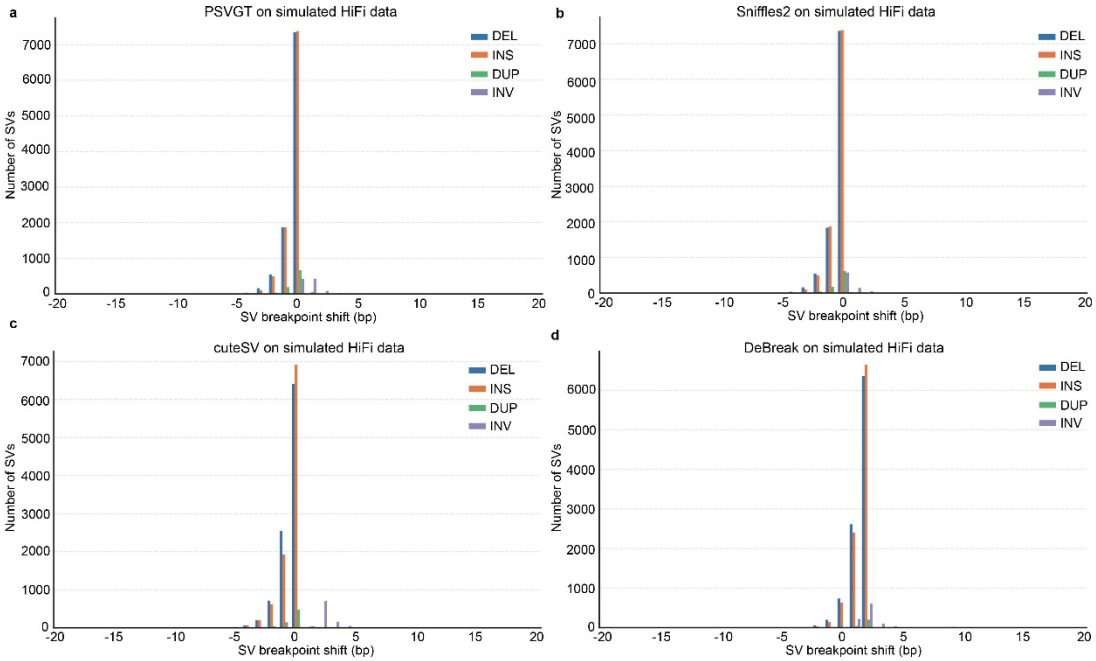

Supplementary Figure 7. **Breakpoint accuracy of SVs detected from HiFi datasets. a-d,** Breakpoint accuracy for PSVGT **(a)**, Sniffles2 **(b)**, cuteSV **(c)**, and DeBreak **(d)**. SVs with breakpoint shift ≤ 20 bp are displayed.

a

Chr	Pos	SV Type	SV size	Tool
20	56,549,947	<INS>	2,287	dipcall
20	56,549,947	<INS>	1,135	SVIM-asm
20	56,549,947	<INS>	1,143	PSVGT

b

Chr	Pos	SV Type	SV size	Tool
22	31,751,841	<INS>	1,337	dipcall
22	31,751,841	<INS>	667	SVIM-asm
22	31,751,841	<INS>	668	PSVGT

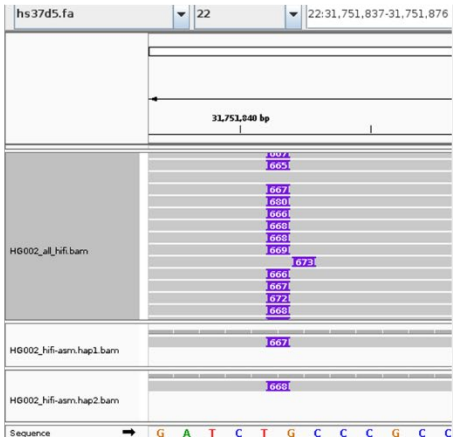

Supplementary Figure 8. Comparison of insertion detection from phased diploid assemblies.
a, Insertion calls on chromosome 20 reported by dipcall, SVIM-asm, and PSVGT, visualized in IGV.
b, Insertion calls on chromosome 22 reported by dipcall, SVIM-asm and PSVGT, visualized in IGV.

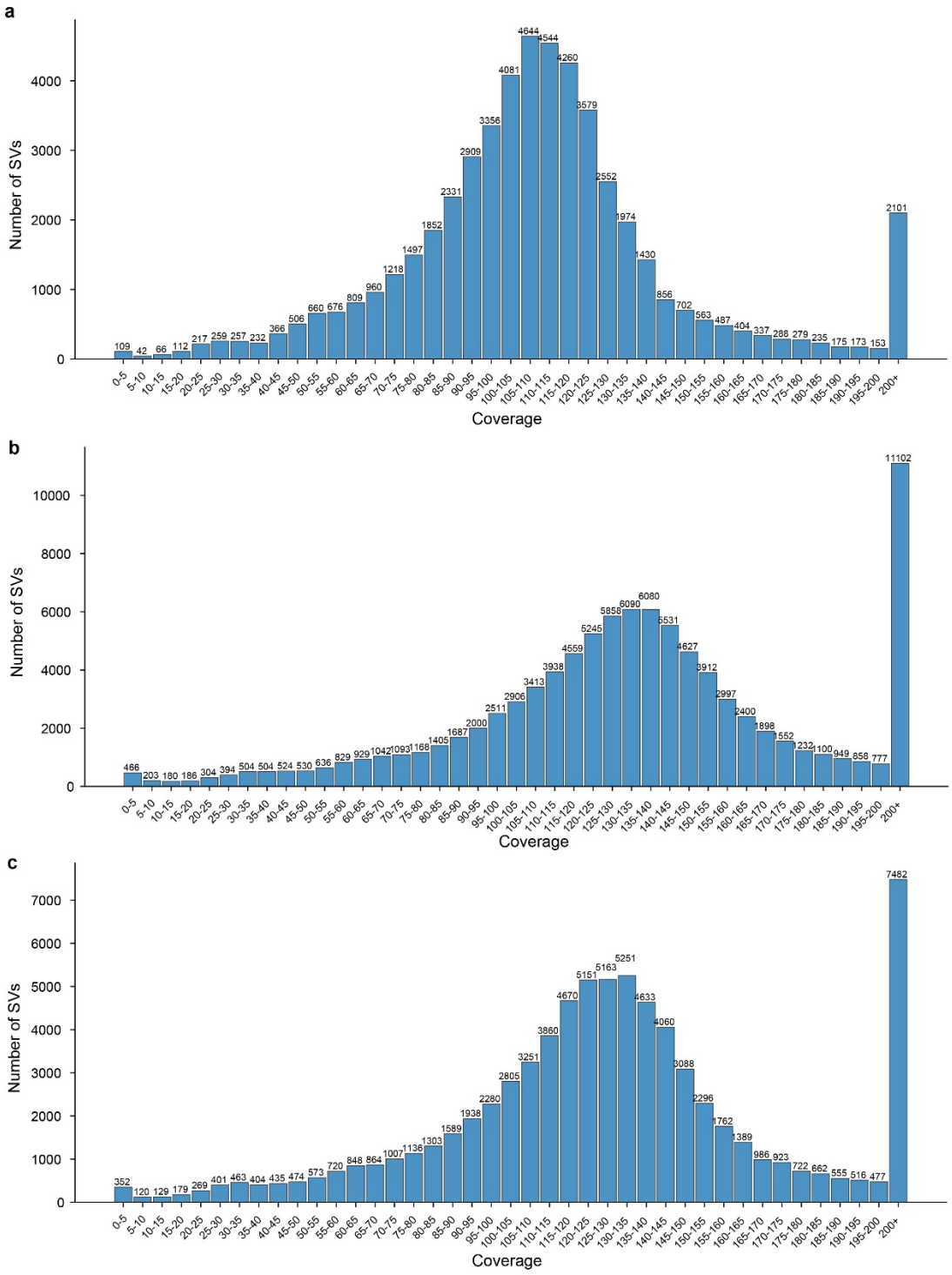

Supplementary Figure 9. Local coverage distribution of SVs in tetraploid potato samples. a-c, Local coverage distributions of SVs detected from PacBio HiFi datasets for potato cultivars Eig **(a)**, Flo **(b)**, and BdF **(c)**.

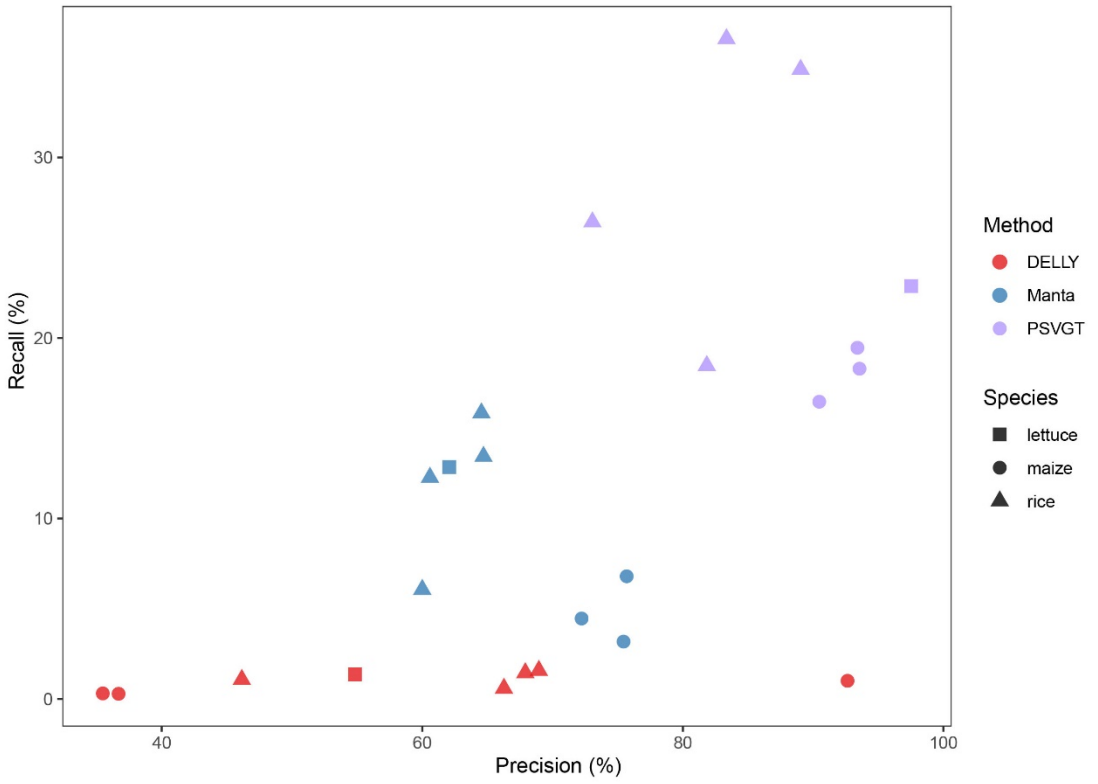

Supplementary Figure 10. Comparison of insertion detection performance from short-read datasets. Eight datasets were evaluated: four from rice, three from maize, and one from lettuce.

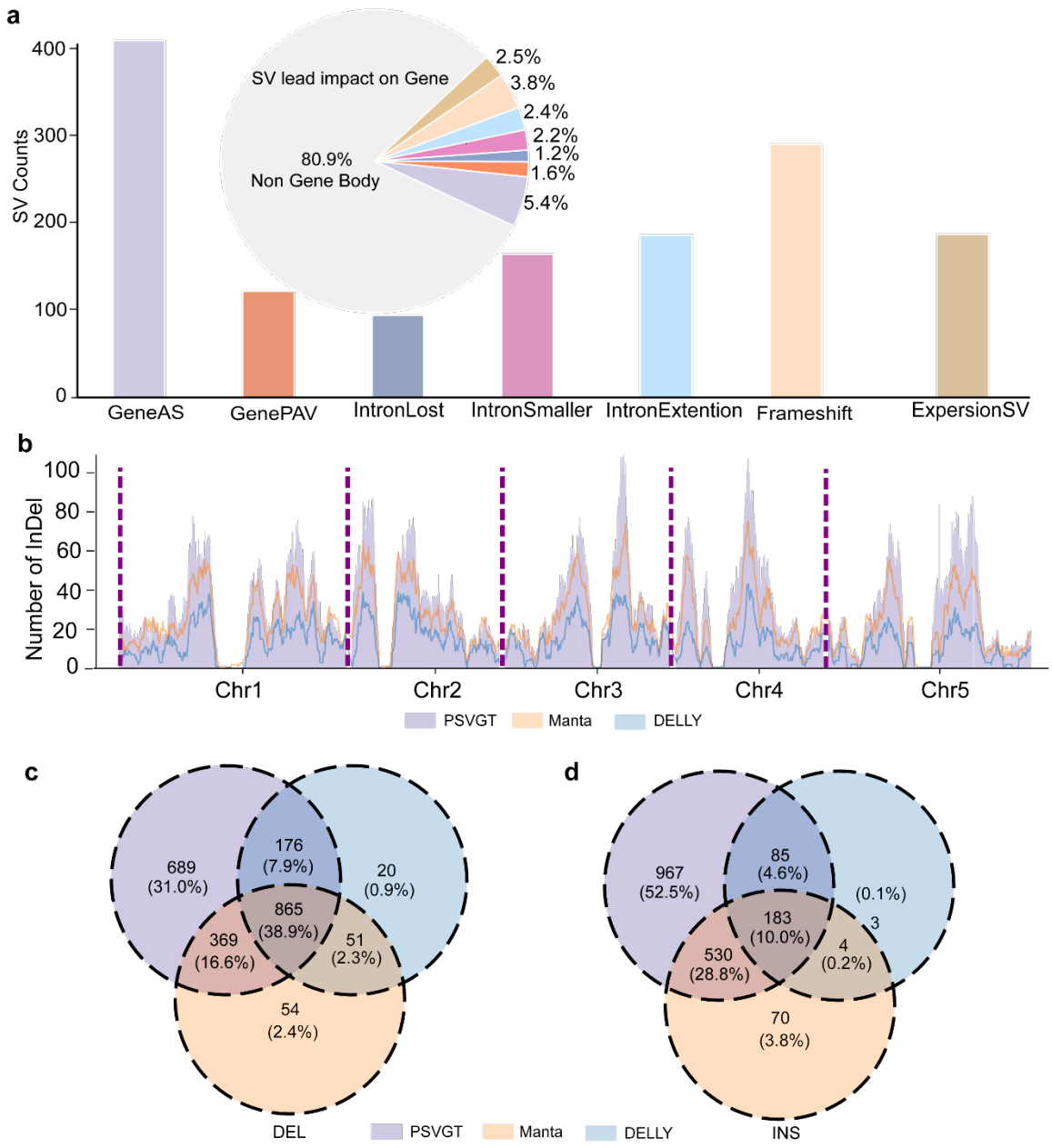

Supplementary Figure 11. SV annotation and marker development module of PSVGT. a, Example annotation of SVs in the PSVGT module. Annotation features are represented by distinct colors. The bar plot indicates the number of SVs annotated under each representative term, while the pie plot displays the proportion of each annotation category. **b,** Density distribution of 50–600 bp InDels across *Arabidopsis* chromosomes. Density curves, color-coded for tools (PSVGT, purple; Manta, orange; DELLY, blue) show the density of InDel number across five chromosomes. **c,d,** Intersection of InDel calls among tools. Venn diagrams showing the number of deletions **(c)** and insertions **(d)** identified by PSVGT, Manta, and DELLY across all eight datasets.